

## Original Article

# Non-invasive quantification of tumor blood flow in prostate cancer using $^{15}\text{O}\text{-H}_2\text{O}$ PET/CT

Lars P Tolbod<sup>1</sup>, Maria M Nielsen<sup>1</sup>, Bodil G Pedersen<sup>2</sup>, Søren Høyer<sup>3</sup>, Hendrik J Harms<sup>1</sup>, Michael Borre<sup>4</sup>, Per Borghammer<sup>1</sup>, Kirsten Bouchelouche<sup>1</sup>, Jørgen Frøkiær<sup>1</sup>, Jens Sørensen<sup>1,5</sup>

<sup>1</sup>Department of Nuclear Medicine and PET Centre, Aarhus University Hospital, Aarhus C, Denmark; Departments of <sup>2</sup>Radiology, <sup>3</sup>Histopathology, <sup>4</sup>Urology, Aarhus University Hospital, Aarhus C, Denmark; <sup>5</sup>Department of Surgical sciences, Nuclear Medicine and PET, Uppsala University, Uppsala, Sweden

Received September 10, 2018; Accepted October 6, 2018; Epub October 20, 2018; Published October 30, 2018

**Abstract:** Tumor blood flow (TBF) measurements in prostate cancer (PCa) provide an integrative index of tumor growth, which could be important for primary diagnosis and therapy response evaluation.  $^{15}\text{O}$ -water PET is the non-invasive gold standard but is technically demanding. The aim of this study was to compare the accuracy of three different non-invasive strategies with an invasively measured arterial input function (BSIF): Using image-derived input functions (IDIF) from either 1) a separate heart scan or 2) the pelvic scan or 3) a populations-based input function (PBIF). Nine patients with biopsy-verified PCa scheduled for prostatectomy were included. All patients were characterized with serum levels of PSA (s-PSA), multiparametric magnetic resonance imaging (mpMRI) and post-surgical histopathology Gleason Grade. Dynamic  $^{15}\text{O}$ -water was performed of the heart and the pelvic area 15 minutes apart. TBF estimated from both wash-in ( $K_1$ ) and wash-out ( $k_2$ ) constants was calculated using a one-compartmental model. Results: Mean (range) s-PSA was 12 (3-27) ng/mL, Gleason Grade Group was 2.9 (1-5),  $k_2$  was 0.44 (0.007-1.2), and  $K_1$  was 0.24 (0.07-0.55) mL/mL/min.  $k_2$  (BSIF) correlated with s-PSA ( $r=0.86$ ,  $P<0.01$ ) and Gleason Grade Group ( $\rho=0.78$ ,  $P=0.01$ ). BSIF, heart-IDIF and PBIF provided near-identical  $k_2$  and  $K_1$  ( $r>0.95$ ,  $P<0.001$ ) with slopes near unity. The correlations of BSIF and pelvic-IDIF rate constants were good ( $r>0.95$ ,  $P<0.001$ ), but individual errors high. In conclusion, non-invasive protocols for  $^{15}\text{O}$ -water PET with IDIF or PBIF accurately measures perfusion in prostate cancer and might be useful for evaluation of tumor aggressiveness and treatment response.

**Keywords:** Tumor blood flow,  $^{15}\text{O}\text{-H}_2\text{O}$ , prostate cancer

## Introduction

Prostate cancer (PCa) is the most common non-skin malignancy in males [1]. The disease is heterogeneous, and the majority of cases are low-risk cancers with slow growth, but a substantial fraction is more aggressive with metastatic potential and PCa accounts for 12% of all cancer mortality in males [2].

The diagnosis and categorical risk-classification of a primary PCa is commonly based on monitoring s-PSA levels, digital rectal palpation and trans-rectal ultrasound (TRUS) guided biopsies. This approach provides a crude estimate of the underlying biology, resulting in a clinical scenario with substantial overtreatment [3].

Consequently, there is a need for more accurate pre-treatment evaluation of the malignant

potential of PCa. Multiparametric magnetic resonance imaging (mpMRI) can be used to localize focal intraprostatic tumors and to guide biopsies for improved histopathology specimens, but does not measure aggressiveness directly [4].

Blood flow is typically increased in more aggressive PCa and imaging with contrast-enhancement provides added value in both TRUS and MRI for functional characterizations [5, 6]. A few studies evaluated absolute quantification of PCa perfusion and found a good agreement towards final post-operative risk scores [7-10]. Absolute quantification of perfusion is technically demanding and is rarely used in clinical practice. However, routinely available access to perfusion data might lead to better informed decisions on therapy and further simplifications of measurements are therefore needed.

## PET perfusion in prostate cancer

**Table 1.** Patient characteristics

| Patient number      | 1    | 2    | 3†   | 4    | 5    | 6     | 7    | 8    | 9    | Mean ± SD |
|---------------------|------|------|------|------|------|-------|------|------|------|-----------|
| Age (yrs)           | 66   | 69   | 76   | 70   | 75   | 67    | 65   | 73   | 69   | 70±4      |
| T category          | pT2c | pT2c | pT3b | pT2c | pT2a | pT2c  | pT2c | pT3a | pT3a |           |
| s-PSA (ng/mL)       | 4.7  | 11.2 | 16.8 | 3.9  | 14.1 | 3     | 7.9  | 26.7 | 17.6 | 11.7±7.8  |
| PIRADS              | 4    | 4    | 5    | 4    | 4    | 4     | 5    | 5    | 5    | 4.4±0.5   |
| Gleason Grade Group | 1    | 2    | 4    | 2    | 5    | 1     | 2    | 4    | 5    | 2.9±1.6   |
| Gleason Score       | 3+3  | 3+4  | 4+4  | 3+4  | 4+5  | 3+3   | 3+4  | 3+5  | 5+4  |           |
| Tumor MVD           | 5.8  | 16.5 | 16.3 | 2.4  | 6.9  | 11.7  | 6.0  | 10.9 | 2.9  | 8.8±5.3   |
| $k_2$               | 0.13 | 0.53 | 0.48 | 0.20 | 0.29 | 0.007 | 0.13 | 1.07 | 1.18 | 0.44±0.45 |
| PTF (mL/mL)         | 0.60 | 0.44 | 0.61 | 0.50 | 0.64 | -     | 1.05 | 0.50 | 0.47 | 0.60±0.21 |
| $K_1$               | 0.08 | 0.23 | 0.30 | 0.10 | 0.18 | 0.07  | 0.14 | 0.54 | 0.55 | 0.24±0.20 |
| $K_1$ (image max)   | 0.17 | 0.45 | 0.45 | 0.18 | 0.30 | 0.14  | 0.25 | 0.75 | 1.05 | 0.42±0.31 |

Gleason Score, Gleason Grade Group and Vessel Density were defined post prostatectomy.  $k_2$ , PTF and  $K_1$  measured using BSIF are shown.  $K_1$  (image max) is the maximum  $K_1$  measured in the tumor on parametric images obtained using BSIF. †HIDIF was used instead of BSIF.

Dynamic positron emission tomography (PET) with  $^{15}\text{O}$ -water is considered the gold standard for non-invasive perfusion measurements in all tissues and has been used to define the accuracy of MRI in PCa perfusion [11].  $^{15}\text{O}$ -water PET is highly reproducible [12, 13] but has remained a research tool due to complex use.

A major obstacle is the need for an invasive arterial line for continuous radioactivity sampling simultaneous with scanning to establish the input function for kinetic modeling. In tissues of the lower thorax and upper abdomen an image-derived input function (IDIF) can substitute invasive blood measurements by measuring radioactivity concentrations directly from images of the left ventricular cavity of the heart or the aorta (HIDIF) [14]. However, due to the low resolution of PET scanners, an IDIF from pelvic arteries (PIDIF) severely underestimates the true blood concentration due to partial volume effect (PVE) leading to an overestimation of blood flow.

The short half-life of  $^{15}\text{O}$  and low radiation dose of  $^{15}\text{O}$ -water exams allow for serial and near simultaneous dynamic imaging of the heart and prostate within the same session. Thus, if infusion of  $^{15}\text{O}$ -water is highly standardized, a HIDIF can be derived from a separate scan and used either directly to substitute arterial blood sampling or to correct a PIDIF by utilizing the relation between cardiac output and the area under the atrial curve [15].

An alternative to IDIFs is population-based methods. Previously, Komar et al [16] has

shown that tumor perfusion imaging in head and neck tumors can be performed using a population-based input function (PBIF) normalized by body surface area. However, the accuracy of the method was limited by lack of infusion standardization in the study.

The aim of this study was therefore to investigate the feasibility and accuracy of non-invasive protocols based on IDIFs and PBIF for routine quantification and visualization of PCa perfusion in using  $^{15}\text{O}$ -water PET with arterial blood sampling as the gold standard.

### Methods

Nine patients were enrolled in this study between January 2014 and November 2014, consecutively included from The Department of Urology at Aarhus University Hospital and referred for radical prostatectomy. All had newly detected PCa assessed by s-PSA levels, digital rectal examination, endorectal ultrasonography, and standardized TRUS biopsies. Inclusion criteria were biopsy-proven PCa, planned surgical intervention and no contraindications to 3 Tesla mpMRI. Patient characteristics are shown in **Table 1**. The patients underwent PET at least eight weeks after biopsy to avoid imaging artefacts after TRUS biopsy. None were treated with antiandrogen medication. The protocol was approved by the Central Denmark Region Committees on Health Research Ethics (M-2013-59-13) and all subjects signed a written informed consent to participate.

### *Imaging*

All patients, except patient 6, underwent PET and mpMRI scans on the same day. PET and mpMRI were 19 days apart for patient 6. The order of the scans varied between patients.

**PET:**  $^{15}\text{O}$ -water scans were performed on a Siemens Biograph Truepoint PET/CT scanner. Two PET/CT scans were performed in each patient. One scan covering the heart (6 min dynamic scan with 22 frames (1×10 s, 8×5 s, 4×10 s, 2×15 s, 3×20 s, 2×30 s, 2×60 s)), and one covering the pelvis (7 min dynamic scan with 32 frames (1×10 s, 18×5 s, 4×10 s, 2×15 s, 3×20 s, 2×30 s, 2×60 s)). A bolus injection of  $^{15}\text{O}$ -water (400 MBq) at the beginning of each scan was performed using a MedRad Contrast Infusion pump (1 ml/s), followed by infusion of 30 mL saline. Heart rate and systolic blood pressure was measured 1 min before and after the injection. Arterial blood sampling from a radial artery was performed using an automatic blood sampler (Allogg ABSS, Allogg AB, Sweden) during both scans. Data was corrected for delay and dispersion by fitting the early part of the sampler curve to the PIDIF using the method of van den Hoff et al [17]. A low dose CT was performed prior to the scans for attenuation correction. All standard corrections were applied. Cardiac images were reconstructed according to the institution's standard protocol for  $^{15}\text{O}$ -water cardiac perfusion [18]. Pelvic images were reconstructed using a 3D OSEM algorithm in a 2×2×2 mm matrix.

**mpMRI:** All mpMRI examinations were performed with a 3 Tesla magnet, Siemens Skyra (Siemens, Erlangen, Germany) with an 18-channel body-phased array coil. Sagittal T2-weighted images of the pelvis were obtained together with high resolution axial and coronal T2 weighted images (T2w) of the prostate. Diffusion weighted images (DWI) of the prostate with b-values 0, 50, 400 and 800 were obtained and apparent diffusion coefficient (ADC) map and calculated b=1400 images were constructed.

All lesions that could possibly explain an elevated PSA level were scored according to the PIRADS (prostate imaging reporting and data system) classification version 1 [19].

**Immunohistochemistry:** Robot-assisted radical prostatectomy was performed within one month of imaging (median 10 days, range 2-29 days). The tissue was processed using standard techniques evaluated according to international guidelines. Carcinomas were outlined, measured and assigned a Gleason score according to the ISUP 2005 definition [20] and grouped into Gleason Grade Groups [21]. The sections with the highest Gleason scores were selected for immunohistochemistry to estimate microvascular density (MVD) using CD34-DAB staining [22].

### *Image analysis*

T2w MRI volumes were fused with the low dose CT volumes, and consequently PET volumes, using rigid normalized mutual information [23] as implemented in the Carimas software [24] (v2.7, Turku PET Centre, Finland). Using Carimas, regions of interest (ROIs) were drawn directly on the T2w MRI based on the delineation of tumor and glandular regions (peripheral and transition zones) using both T2w and DWI images, and PET time activity curves (TACs) were extracted. Small corrections (translation of ROIs) for deformation of the prostate between PET and MRI (typically due to differences in bladder and rectal filling) were performed on 2 patients. An example of a dynamic PET-series is shown in [Figure S4](#) in the supplementary information.

IDIFs were extracted automatically from the dynamic PET volumes (PIDIF and HIDIF) using cluster analysis previously described by Harms et al [25]. The HIDIF cluster was eroded by two pixels and the PIDIF by one pixel. The HIDIF was delay-corrected using the method of van den Hoff et al [17]. The area under the curve of the first-pass peak was calculated as described previously [15]. In addition to the raw HIDIF and PIDIF, a HIDIF corrected for differences in systolic blood pressure (HIDIF\_sBT, [Figure S5](#)) and a PDIF corrected for PVE using the AUC ratio between HIDIF\_sBT and PIDIF (PIDIF\_AUC) were created.

A population-based input function was constructed from all BSIFs using the method of Komar et al [16] in which body surface area normalized BSIFs are averaged. Individual dispersion and delay-correction was performed on the PBIF again using the van den Hoff method.

## PET perfusion in prostate cancer

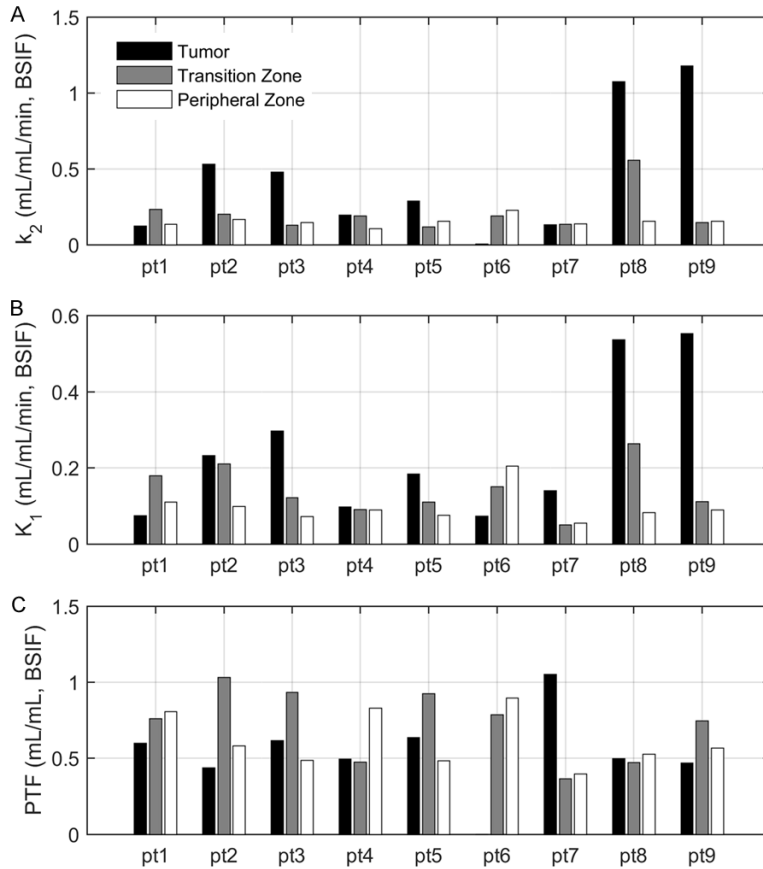


**Figure 1.** A and B: Blood flow measured by both  $K_1$  or  $k_2$  was elevated in all tumors with Gleason Score 3+4 or greater relative to the peripheral and transition zone. However, for patient 7, only  $K_1$  was elevated and  $k_2$  is the same level as the surrounding tissue. C: The perfusable tissue fraction (PTF) tended to be lower in tumor compared to reference tissues, however, the difference was not statistically significant.

$^{15}\text{O}$ -water data were analyzed using a standard one-tissue compartment model:

$$C_{PET}(t) = K_1 e^{-k_2 t} \otimes C_A(t + \Delta T)$$

With three fitting parameters:  $K_1$ ,  $k_2$  and  $\Delta T$  [14]. The perfusable tissue fraction (PTF, unit mL/mL) was calculated as  $K_1/k_2$ .

Parametric  $k_2$  and  $K_1$  images were created using the basis function method [25]. Wash-out images ( $k_2$ ) are expected to be inaccurate in regions with low wash-in signal (ie regions with very low flow). To remove the noisy appearance in the very low flow regions, a mask was first created from the  $K_1$  image prior to post-filtering (setting values below 0.13 to zero) and imposed on the  $k_2$  image. Then, a  $3 \times 3$  median filter was applied to remove spikes from the image. Finally, a 5 mm 3D Gaussian post-filter was

applied to both  $k_2$  and  $K_1$  images. To estimate the agreement between the parametric images and values based on fitting of ROI-averaged TAC, the maximum  $K_1$  voxel value at the tumor site (identified using either thresholding (40% 3D VOI, Hybrid Viewer 1.4, Hermes Medical, or manual search using a 1 cm circular ROI) was compared to  $K_1$  obtained from fitting ROI-averaged TAC.

### Statistical analysis

Correlation and differences between TBF measures ( $k_2$  and  $K_1$ ) and PTF values established with the different input functions (BSIF, IDIFs and PBIF) were analyzed using linear regression analysis. For equivalent measures, the range of errors was reported). Linear regression analysis was also used to analyze correlation between TBF and the continuous measures of s-PSA and MVD. Correlations between  $k_2$  and Gleason Grade Group were evaluated using Spearman's rank analysis.

A two-sided  $P$ -value  $< 0.05$  was considered statistically significant. Analyses were performed in JMP 13 (SAS Institute).

## Results

### TBF correlates with s-PSA and Gleason Grade Group

The blood sampler failed during one scan in patient 3 and BSIF was substituted with the HIDIF for calculation of perfusion in the pelvic region. Tumor perfusion in one patient (patient 6) was too low to obtain a reliable estimate of PTF and this value was consequently discarded.

TBF estimated from  $k_2$  was higher than  $K_1$  estimated from wash-in rates ( $P < 0.05$ , see **Table 1**). **Figure 1** compares TBF estimated from both

**Table 2.** Correlations for perfusion measures

|         |                   | Linear fit equation | Error Range    | r      | P       |
|---------|-------------------|---------------------|----------------|--------|---------|
| $K_1$   | $K_1$ (HIDIF)     | 1.24x-0.01          | [0.01; 0.13]   | 0.99   | <0.0001 |
| $K_1$   | $K_1$ (HIDIF_sBT) | 1.04x+0.00          | [-0.01; 0.02]  | 0.99   | <0.0001 |
| $K_1$   | $K_1$ (PIDIF)     | 4.61x-0.14          | [0.08; 2.21]   | 0.95   | <0.0001 |
| $K_1$   | $K_1$ (PIDIF_AUC) | 1.07x-0.00          | [-0.01; 0.03]  | 0.99   | <0.0001 |
| $K_1$   | $K_1$ (PBIF)      | 1.03x-0.00          | [-0.06; 0.09]  | 0.98   | <0.0001 |
| $K_1$ † | $K_1$ (image MAX) | 1.59x+0.03          | [0.07; 0.50]   | 0.97   | <0.0001 |
| $k_2$   | $k_2$ (HIDIF)     | 0.96x+0.02          | [-0.04; 0.13]  | 0.99   | <0.0001 |
| $k_2$   | $k_2$ (PIDIF)     | 1.27x+0.02          | [-0.01; 0.41]  | 0.98   | <0.0001 |
| $k_2$   | $k_2$ (PBIF)      | 1.04x-0.02          | [-0.15; 0.06]  | 0.99   | <0.0001 |
| $k_2$   | $K_1$             | -                   | -              | 0.99   | <0.0001 |
| $k_2$ † | s-PSA             | -                   | -              | 0.86   | <0.01   |
| $k_2$ † | MVD               | -                   | -              | 0.02   | 0.96    |
| PTF     | PTF (HIDIF_sBT)   | 0.72x+0.13          | [-0.20; 0.33]  | 0.85   | <0.0001 |
| PTF     | PTF (PIDIF_AUC)   | 0.62x+0.09          | [-0.47; -0.05] | 0.72   | 0.0001  |
| PTF     | PTF (PBIF)        | 1.23x-0.05          | [-0.15; 0.68]  | 0.80   | <0.0001 |
|         |                   |                     |                | $\rho$ | P       |
| $k_2$ † | GG                | -                   | -              | 0.78   | 0.01    |
| $K_1$ † | GG                | -                   | -              | 0.82   | <0.01   |

Correlation between perfusion measures obtained using input functions from a blood sampler (BSIF) and image derived input functions (IDIF, H: heart, P: pelvic) as well as tumor characteristic parameters. Unless otherwise stated, the perfusion measure is derived using BSIF. For continuous variables, Pearson correlation coefficient, r, and its significance, P, is given. For ordinal variables, Spearman's rank correlation coefficient,  $\rho$ , and its significance, P, is given. For equivalent measures, the error range is also shown. †Only tumor is included.

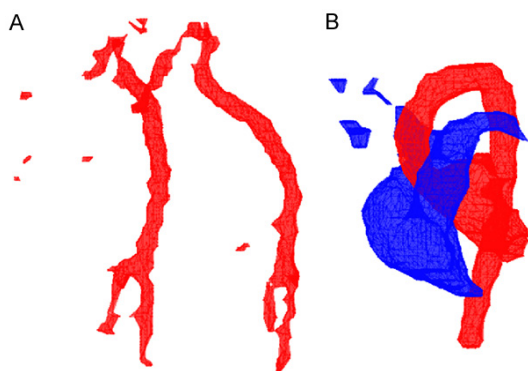


**Figure 2.** Typical blood voxels identified by the cluster analysis (patient 6) for the extraction of IDIFs. (A) The pelvic field of view with the arterial cluster in red, (B) the heart field of view with the arterial cluster in red. In the heart, venous blood arriving to the right heart is identified as the blue cluster.

$k_2$  and  $K_1$  and PTF in tumor and surrounding tissue. TBF was generally higher in tumor tissue compared to non-tumorous tissue in both the

peripheral and transitional zone for tumors with post-operative Gleason Score 3+4 or greater. However, patient 7 (GS 3+4) was an exception as only  $K_1$  was greater in the tumor compared to the surrounding tissue. Elevated  $K_1$  in the transition zone, consistent with BPH, was found in 4 patients, however, due to high PTF in the transition zone compared to the tumor, the elevation was only manifested in  $k_2$  in one patient. Though there seems to be a tendency of lower PTF in the tumor compared to surrounding tissue, it was not statistically significant.

TBF correlated with both s-PSA and Gleason Grade Group (Table 2). No significant correlations with PTF were found. No correlation between TBF and MVD was found. In fact, MVD was not found to correlate with any perfusion measure, s-PSA ( $r=0.31$ ,  $P=0.41$ ) nor Gleason Grade Group ( $r=-0.05$ ,  $P=0.89$ ) in this patient group.

*TBF can be measured using IDIFs*

Typical clusters used for extracting IDIFs are shown in Figure 2 and all input functions for the 9 patients are shown in Figure 3. In most of the patients, the AUC-corrected PIDIF had too high activity during late time frames. In some patients this was associated with a high peak PIDIF, suggesting that the AUC correction was inaccurate, but it is very likely that spill-in from other tissues also contributes to this observation. In contrast, the mean peak height difference between HIDIF and BSIF was not different from zero, just as no spill-in was observed at longer times. An injection anomaly occurred during the heart scan of patient 2 and the HIDIF of this patient was consequently discarded. Linear regression and Bland-Altman plots are shown for all used combinations of input functions in Figures S1, S2, S3 in the suppl. material and summarized in Table 2.

An excellent correlation between TBF derived from BSIF and HIDIF was found. Linear regression revealed a slope close to unity for  $k_2$ , but slightly higher for  $K_1$  (1.24). Maximum error

## PET perfusion in prostate cancer

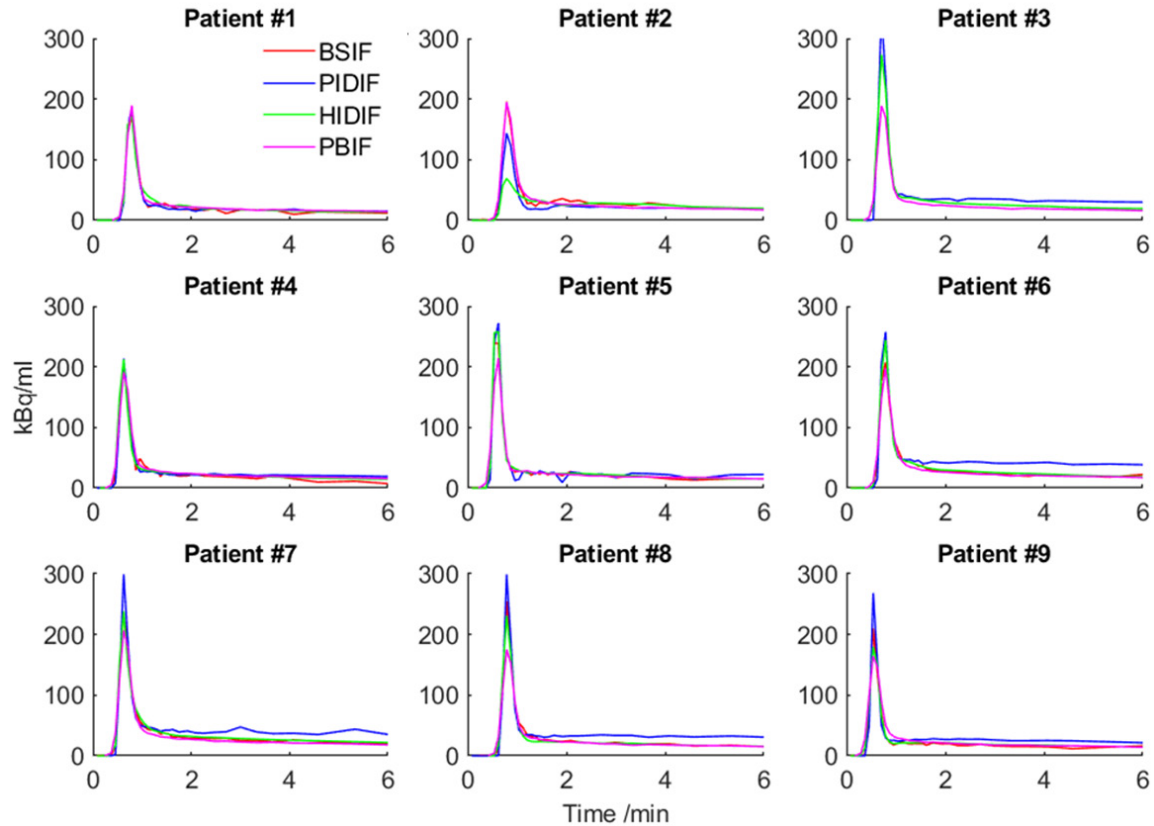


**Figure 3.** Input functions for all 9 patients. Input functions derived from arterial blood sampling (BSIF with delay and dispersion correction), the heart field of view (HIDIF with delay and sBT correction), the pelvic field of view (PIDIF with AUC correction) and the population-based input function (PBIF with delay and dispersion correction). In patient 2, an injection anomaly for the heart scan was observed (peak small and broad). For patient 3, the arterial blood sampling failed, and the curve is not shown.

ranges were -0.04 to 0.13 and -0.01 to 0.13, respectively. However, differences in  $K_1$  was partly explained by differences in systolic blood pressure (sBT) between the two scans. Correcting for blood pressure effects on the area under the first pass curve using a linear model (Figure S5) changed the slope to unity and reduced the error range to -0.01 to 0.02. As expected, the uncorrected PIDIF overestimated both  $k_2$  (slope: 1.27) and  $K_1$  (slope: 4.6). However, correcting the PIDIF by normalizing the area under the first-pass curve to that of the HIDIF (corrected for blood pressure effects), resulted in a slope of unity for  $K_1$ , but did not affect  $k_2$ . The maximum error range for PIDIF was similarly reduced for  $K_1$  (-0.01 to 0.03), but still large for  $k_2$  (-0.01 to 0.41). In this case, the error associated with  $k_2$  is likely to be due to spill-in in the pelvic arteries. PTF estimated with both corrected HIDIF and PIDIF correlated well with BSIF, however, large individual errors were observed.

### TBF can be measured using PBIF

Similar to the IDIFs, dispersion corrected PBIFs are shown in Figure 3. As expected, the PBIF did not appear as noisy as the individual BSIFs and, just as observed for the HIDIF, the mean peak height difference between PBIF and BSIF was not different from zero and no spill-in was observed at longer times. Linear regression yielded a slope close to unity for both  $K_1$  and  $k_2$  with a slightly larger spread of errors. PTF was generally underestimated using PBIF and, as for the IDIFs, large individual errors were observed.

### Parametric Images were quantitative

Parametric  $K_1$  and  $k_2$  images fused with MRI T2 images are shown in Figure 4 for four selected patients. Images of  $k_2$  were noisy, and, in most cases, the tumor could not be delineated by the 40% threshold method. However, tumor delin-

## PET perfusion in prostate cancer

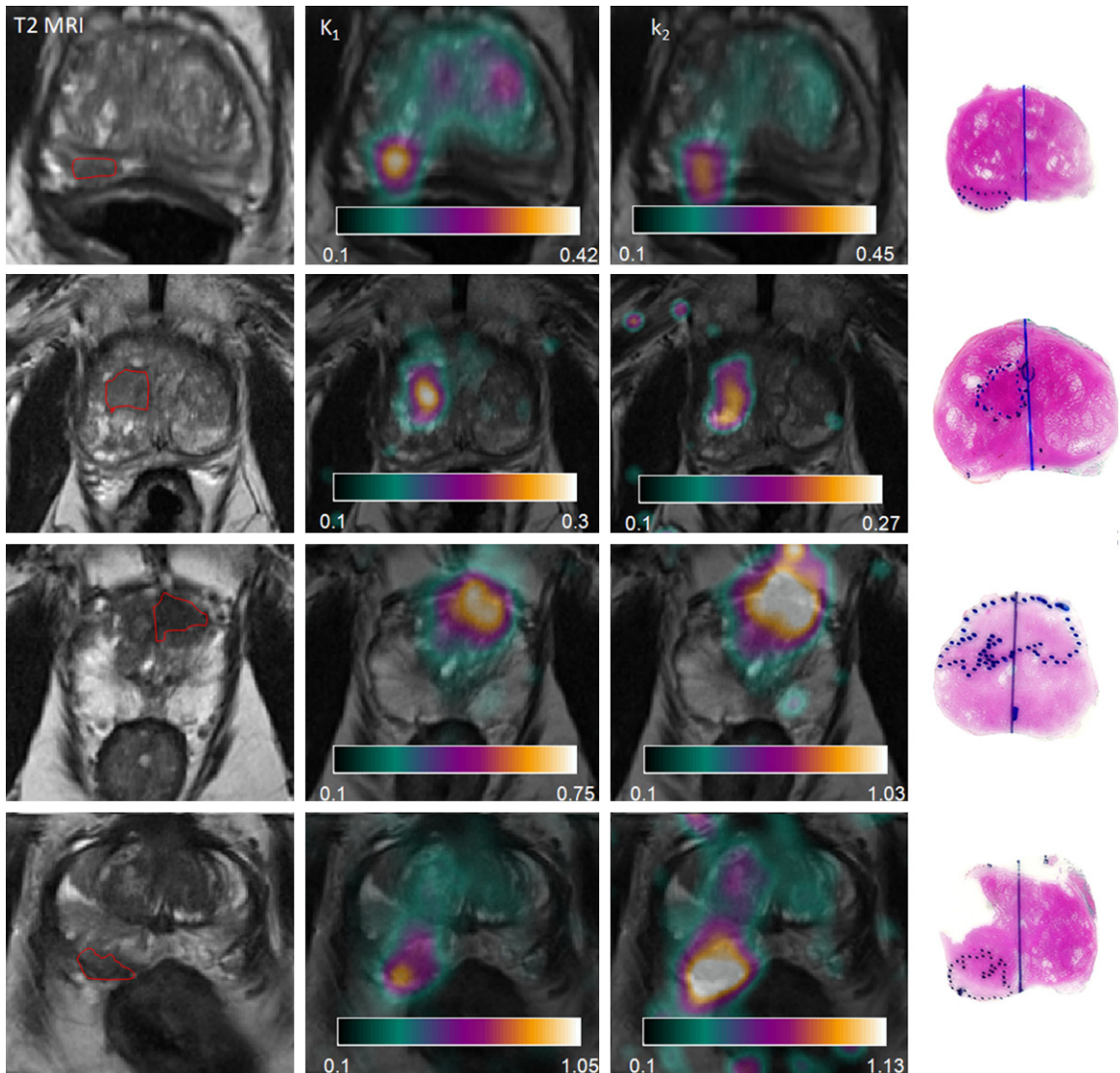


**Figure 4.** T2w MRI, parametric  $K_1$  and  $k_2$  images and pathology for 4 selected patients. Tumor regions identified by radiologist are indicated on the MRI images. From the top: Patient 2 with posterior carcinoma in the peripheral zone, patient 5 with carcinoma in the right side of the transition zone, patient 8 with large anterior carcinoma and patient 9 with posterior carcinoma in the peripheral zone. In patient 9, increased flow is seen ventral to the tumor most likely reflecting post-TRUSbx inflammation or bleeding sequela. Alignment between pathology and imaging is approximate.

eation was successful in 6 out of 9 patients using  $K_1$  images. In two cases, flow in the tumor was lower than the surrounding tissue (patients 1 and 6).

Excellent correlations between the maximum value obtained from parametric  $K_1$  images and  $K_1$  and  $k_2$  derived from tumor ROIs were found.

### Discussion

This study investigated the accuracy of simplified protocols for perfusion measurements of

the prostate with  $^{15}\text{O}$ -water PET in patients with primary PCa. The main results of the study demonstrated that tumor blood flow can be measured reliably using  $^{15}\text{O}$ -water without invasive arterial blood sampling even in regions without large arteries in the scanning field-of-view, and that true perfusion with  $^{15}\text{O}$ -water PET in PCa is highly correlated with both s-PSA and histopathology. The use of an IDIF from a separate cardiac scan provides accurate perfusion estimates, thereby reducing the invasiveness associated with arterial lines. PIDIF might

simplify the procedure even further but limits the accuracy.

Very few studies have applied  $^{15}\text{O}$ -water PET in prostate pathologies. Prostate perfusion was first measured using  $^{15}\text{O}$ -water PET and a 1-compartmental model by Inaba in 1992 [26] in a study in which prostate perfusion in 11 PCa patients with advanced PCa was compared to nine normal volunteers and six patients with benign prostate hypertrophy (BPH). The study demonstrated that PCa tumor perfusion was  $0.29 \pm 0.08$  ml/min/g, which was significantly higher than in normal prostate and BPH. Perfusion values in normal prostate tissue correlated negatively with age. In a subsequent study, Muramoto et al [11] studied six patients with known PCa with  $^{15}\text{O}$ -water using an autoradiographic technique. TBF was  $0.55 \pm 0.29$  ml/min/g. Arterial blood sampling was used in both studies. Kurdziel et al [27] studied the effect of anti-angiogenic therapy in androgen independent PCa in 6 individuals using a wash-out model and a descending aorta derived input function (manually-drawn) with no blood sampler validation. Mean pretreatment TBF was 0.78 mL/min/g and the change in TBF after therapy was found to correlate with the change in s-PSA.

In the current study, perfusion was measured using a kinetic model that parameterizes both wash-in ( $K_1$ ) and wash-out ( $k_2$ ) of water.  $k_2$  measures a flow weighted average and, in the case of binary flow distribution, only reflects perfusion in the perfused part of the tumor and is virtually free of PVE even for small tumors [14, 28]. Consequently,  $k_2$  ( $0.44 \pm 0.45$  mL/min/mL) was found to be significantly higher than  $K_1$  ( $0.24 \pm 0.20$  mL/min/mL). These numbers are consistent with previous studies [11, 26, 27]. PTF, the ratio of  $K_1/k_2$ , was generally lower in tumors compared to the surrounding tissue (Figure 1). Though, in this small cohort where 2 of 9 tumors were low grade (3+3) and 4 patients had elevated flow in the transition zone due to BPH, the difference in PTF between tumor and surrounding tissue did not reach statistical significance. In patient 6, the TBF was very low, causing PTF to be fitted at substantially above the physiological upper limit of 1. A lower PTF in more aggressive and larger cancers suggests that a substantial fraction of the tumor volume is underperfused, for which there are several potential explanations such as high interstitial

pressure [14], large blood pool, fibrosis and necrosis. The mean tumor PTF was  $0.60 \pm 0.21$  ml/ml, which again is in line with the study by Inaba [26] ( $0.59 \pm 0.05$  ml/ml), but also with the finding in liver and lung metastases by Lubberink et al [14] ( $0.60 \pm 0.12$  ml/ml).

TBF, as measured using the methods presented here, correlated with tumor Gleason Grade. This is not surprising, since Gleason Grade is a strong indicator of aggressiveness and growth. Moreover, TBF performed before treatment reflects the momentary metabolic needs of the tumor. From a clinical point of view, the combination of a simplified scanning procedure with less invasiveness and automated formation of parametric images might allow  $^{15}\text{O}$ -water PET to be used for rapid assessment of tumor growth and response to therapy.

The correlation of TBF of  $^{15}\text{O}$ -water towards s-PSA was high. Positive correlations of TBF towards s-PSA were previously shown using dynamic contrast-enhanced CT (DCE-CT) [8] and with DCE-MR [29]. Hence, the data from this study underscores that s-PSA is strongly proportional to TBF at least in localized disease. To what extent TBF adds incremental value to s-PSA measurements remains to be shown.

MVD did not correlate to any aspect of PET, s-PSA or Gleason Grade Group in this study. Though CD34-MVD is often used as a marker of angiogenesis in PCa, results are ambivalent as documented in a recent review [30]. Similar to the current study, Huellner et al [7] failed to find a correlation between contrast-enhanced CT derived TBF and MVD in a cohort of 32 intermediate and high grade PCa.

One of the main obstacles for measuring TBF using  $^{15}\text{O}$ -water PET is the accurate acquisition of an arterial input function. For imaging outside of the thorax and upper abdomen, an arterial line for blood sampling is generally needed unless a model-based PVE correction is applied [31]. In this study, we show how perfusion can be measured without an arterial line using either IDIFs derived from a separate scan of the heart or a population-based input function.

Comparing results using BSIF and heart-IDIF (HIDIF) both  $k_2$  and  $K_1$  have slopes close to one (Table 2). The area under the curve (AUC) of the

first pass, corrected for partial volume effects, is directly proportional to cardiac output throughout the system [15, 32], and, consequently, the IDIF changes with cardiac work. As the HIDIF is acquired 15 min before the pelvic scan changes in hemodynamic conditions must be accounted for. The relative change in AUC between the scans was best explained by the ratio of systolic blood pressures, and a linear model (Figure S5) could be used to correct the HIDIF and increase the accuracy of  $K_1$  measurement. The dual-scan technique should be directly applicable in other non-thoracic regions (e.g. brain) but requires more validation studies. The total radiation dose of the additional scan is low and amounts to 0.5 milliSievert, including low-dose CT on a modern scanner.

Correlations of perfusion values for BSIF and pelvic artery IDIF (PIDIF) were surprisingly good. The wash-in rate  $K_1$  was overestimated by a factor of almost 5, which was introduced by a reciprocal amount of partial volume effect on the PIDIF. However, when correcting for PVE-induced differences in AUC between HIDIF and PIDIF (including the sBT correction on the HIDIF), the slope was reduced to unity and the accuracy greatly improved. For  $k_2$  derived with a PIDIF a slight overestimation with a factor 1.3 was seen, illustrating that wash-out is virtually free of PVE. The overestimation is likely due to effects of spill-in effects on the PIDIF at longer times and might be reduced using a background model [31]. Nevertheless, the individual errors for the PIDIF approach remained higher for both  $K_1$  and  $k_2$  compared to the HIDIF approach and, unless cardiac output is determined reliably from a non-PET scan, the cardiac scan is needed to correct the PIDIF in which case the HIDIF approach is preferred.

A different one-scan approach is using population-based input functions. Komar et al suggested a method normalizing the BSIF to body surface area [16] and showed that reasonable blood flow results, though with considerable individual variation, can be obtained in the head and neck region. We adapted this method but imposed the strict standardization of the  $^{15}\text{O}$ -water infusion also applied in the dual scan approach. Compared to Komar et al, significant better correlations with BSIF were found and slopes were close to unity for both  $K_1$  and  $k_2$ . The individual error was only slightly larger than observed for the HIDIF approach. However, the

use of the PBIF should be further examined in a larger cohort where the groups for establishing and testing the PBIF are separated.

Previous studies producing parametric  $^{15}\text{O}$ -water images within the field of cardiology have shown that wash-out images are subject to false noise-induced high flow values outside the heart and that PTF and blood pool images can be used to mask-out these regions [25]. The results of the present study demonstrated that this is indeed also true for tumor imaging. Using the  $K_1$  image as a mask instead of PTF, image noise was effectively suppressed in low flow regions of the TBF image (Figure 4). In most patients, the tumor could be outlined directly on  $K_1$  parametric images.  $K_1(\text{max})$  in parametric images correlated well with  $K_1$  and  $k_2$  calculated from ROI-based analysis using carefully drawn ROIs on MRI. As shown in Figure 4 tumor localization with both  $k_2$  and  $K_1$  images corresponds well to both MRI images and histopathology specimens.

### Conclusion

Tumor blood flow can be measured reliably using  $^{15}\text{O}$ -water without invasive arterial blood sampling even in regions without large arteries in the scanning field-of-view. A dual scan strategy in which the input function is derived from a scan of the heart maintains accuracy of TBF for both wash-in and wash-out estimates. With a single scan, a populations-based approach was preferred over IDIFs. Parametric images of TBF provide simplified access to absolute quantification and tissue characterization. This might increase the opportunity for studies of TBF in all PET-centers with access to cyclotrons.

### Acknowledgements

This study was supported by grants from the Danish Cancer Society ("Knæk Cancer") and Aarhus University. The project protocol was approved by the Committee of Health Research Ethics of the Central Danish Region (De Videnskabetiske Komitéer for Region Midtjylland, project-ID: M-2013-59-13).

Informed consent was obtained from all individual participants included in the study.

### Disclosure of conflict of interest

None.

**Address correspondence to:** Lars P Tolbod, Department of Nuclear Medicine and PET Centre, Aarhus University Hospital, Aarhus C, Denmark. ORCID: 0000-0002-8105-7046; E-mail: larstolb@rm.dk

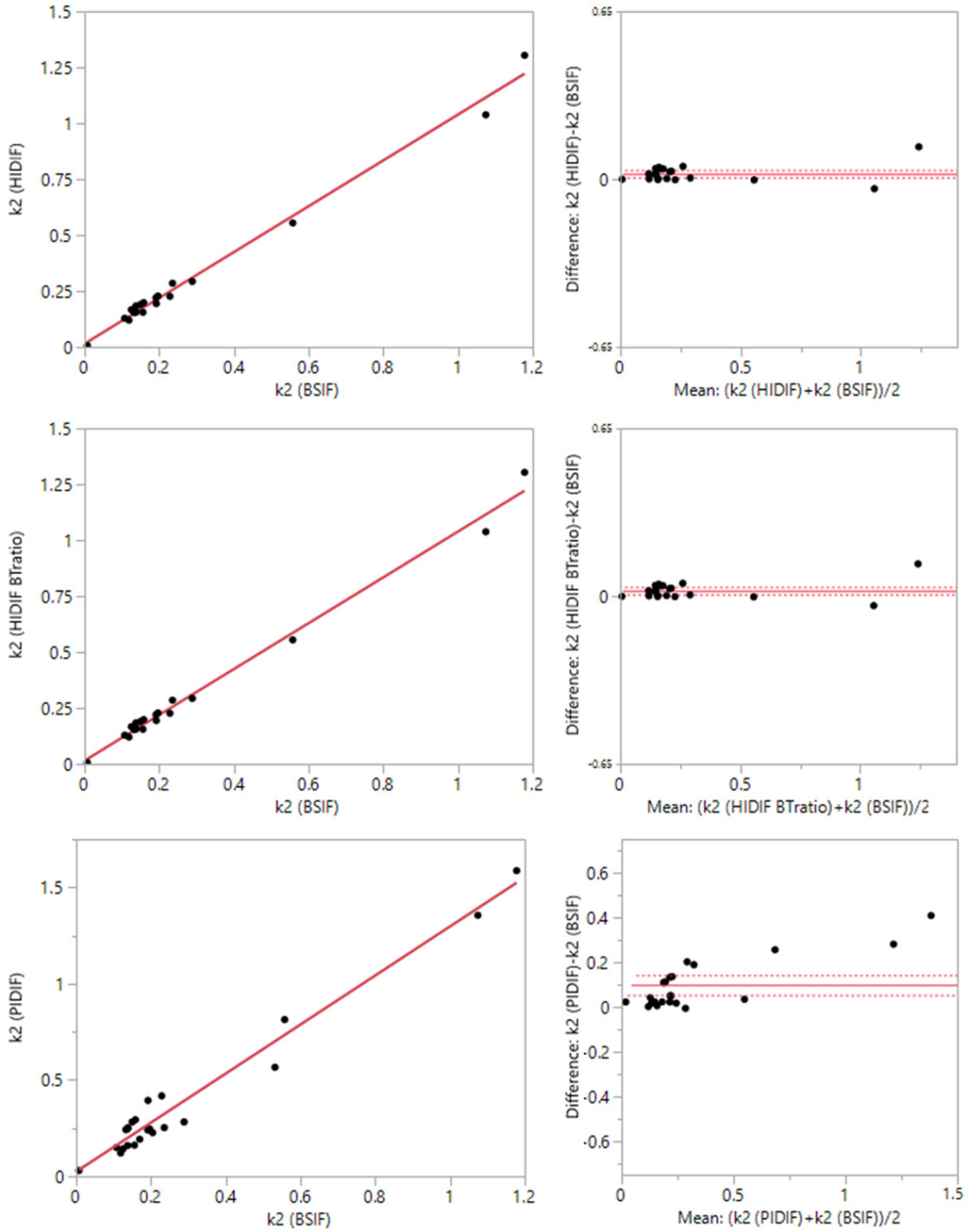
**References**

- [1] Damber JE and Aus G. Prostate cancer. *Lancet* 2008; 371: 1710-1721.
- [2] Global Cancer Facts & Figures 3rd Edition, American Cancer Society, 2015, <http://www.cancer.org/acs/groups/content/@research/documents/document/acspc-044738.pdf>, Accessed: 12/21 2015.
- [3] Loeb S, Bjurlin MA, Nicholson J, Tammela TL, Penson DF, Carter HB, Carroll P and Etzioni R. Overdiagnosis and overtreatment of prostate cancer. *Eur Urol* 2014; 65: 1046-1055.
- [4] Valerio M, Willis S, van der Meulen J, Emberton M and Ahmed HU. Methodological considerations in assessing the utility of imaging in early prostate cancer. *Curr Opin Urol* 2015; 25: 536-542.
- [5] Barrett T, Turkbey B and Choyke PL. PI-RADS version 2: what you need to know. *Clin Radiol* 2015; 70: 1165-1176.
- [6] Li H, Xia J, Xie S, Guo Y, Xin M and Li F. Prostate cancer: a comparison of the diagnostic performance of transrectal ultrasound versus contrast enhanced transrectal ultrasound in different clinical characteristics. *Int J Clin Exp Med* 2015; 8: 21428-21434.
- [7] Huelner MW, Pauli C, Mattei A, Ross S, Diebold J, Vosbeck J, Allgayer B, Strobel K and Veit-Haibach P. Assessment of prostate cancer with dynamic contrast-enhanced computed tomography using an en bloc approach. *Invest Radiol* 2014; 49: 571-578.
- [8] Luczynska E, Heinze-Paluchowska S, Blecharz P, Jereczek-Fossa B, Petralia G, Bellomi M and Stelmach A. Correlation between CT perfusion and clinico-pathological features in prostate cancer: a prospective study. *Med Sci Monit* 2015; 21: 153-162.
- [9] Mitterberger M, Pinggera GM, Horninger W, Bartsch G, Strasser H, Schafer G, Brunner A, Halpern EJ, Gradl J, Pallwein L and Frauscher F. Comparison of contrast enhanced color Doppler targeted biopsy to conventional systematic biopsy: impact on Gleason score. *J Urol* 2007; 178: 464-468.
- [10] Zhao HW, Luo JH, Xu HX, Wang DH, Lai YR, Chen MN, Lv JY, Xie XY, Lu MD and Chen W. The value of contrast-enhanced transrectal ultrasound in predicting the nature of prostate diseases and the Gleason score of prostate cancer by a subjective blood flow grading scale. *Urol Int* 2011; 87: 165-170.
- [11] Muramoto S, Uematsu H, Sadato N, Tsuchida T, Matsuda T, Hatabu H, Yonekura Y and Itoh H. H(2) (15)O positron emission tomography validation of semiquantitative prostate blood flow determined by double-echo dynamic MRI: a preliminary study. *J Comput Assist Tomogr* 2002; 26: 510-514.
- [12] Lodge MA, Jacene HA, Pili R and Wahl RL. Reproducibility of tumor blood flow quantification with 15O-water PET. *J Nucl Med* 2008; 49: 1620-1627.
- [13] van der Veldt AA, Hendrikse NH, Harms HJ, Comans EF, Postmus PE, Smit EF, Lammertsma AA and Lubberink M. Quantitative parametric perfusion images using 15O-labeled water and a clinical PET/CT scanner: test-retest variability in lung cancer. *J Nucl Med* 2010; 51: 1684-1690.
- [14] Lubberink M, Golla SS, Jonasson M, Rubin K, Glimelius B, Sorensen J and Nygren P. 15O-Water PET study of the effect of imatinib, a selective platelet-derived growth factor receptor inhibitor, versus anakinra, an IL-1R antagonist, on water-perfusible tissue fraction in colorectal cancer metastases. *J Nucl Med* 2015; 56: 1144-1149.
- [15] Harms HJ, Tolbod LP, Hansson NH, Kero T, Orndahl LH, Kim WY, Bjerner T, Bouchelouche K, Wiggers H, Frokiaer J and Sorensen J. Automatic extraction of forward stroke volume using dynamic PET/CT: a dual-tracer and dual-scanner validation in patients with heart valve disease. *EJNMMI Phys* 2015; 2: 25.
- [16] Komar G, Oikonen V, Sipila H, Seppanen M and Minn H. Noninvasive parametric blood flow imaging of head and neck tumours using [15O] H2O and PET/CT. *Nucl Med Commun* 2012; 33: 1169-1178.
- [17] van den Hoff J, Burchert W, Muller-Schauenburg W, Meyer GJ and Hundeshagen H. Accurate local blood flow measurements with dynamic PET: fast determination of input function delay and dispersion by multilinear minimization. *J Nucl Med* 1993; 34: 1770-1777.
- [18] Nielsen R, Jorsal A, Iversen P, Tolbod L, Bouchelouche K, Sorensen J, Harms HJ, Flyvbjerg A, Botker HE and Wiggers H. Heart failure patients with prediabetes and newly diagnosed diabetes display abnormalities in myocardial metabolism. *J Nucl Cardiol* 2018; 25: 169-176.
- [19] Barentsz JO, Richenberg J, Clements R, Choyke P, Verma S, Villeirs G, Rouviere O, Logager V, Futterer JJ; European Society of Urogenital Radiology. ESUR prostate MR guidelines 2012. *Eur Radiol* 2012; 22: 746-757.
- [20] Epstein JI, Allsbrook WC Jr, Amin MB, Egevad LL; ISUP Grading Committee. The 2005 international society of urological pathology (ISUP) consensus conference on gleason grading of prostatic carcinoma. *Am J Surg Pathol* 2005; 29: 1228-1242.

## PET perfusion in prostate cancer

- [21] Gordetsky J and Epstein J. Grading of prostatic adenocarcinoma: current state and prognostic implications. *Diagn Pathol* 2016; 11: 25.
- [22] Van Blarigan EL, Gerstenberger JP, Kenfield SA, Giovannucci EL, Stampfer MJ, Jones LW, Clinton SK, Chan JM and Mucci LA. Physical activity and prostate tumor vessel morphology: data from the health professionals follow-up study. *Cancer Prev Res* 2015; 8: 962-967.
- [23] Studholme C, Hawkes DJ and Hill DLG. A normalised entropy measure for multi-modality image alignment. *Proc SPIE* 1998; 3338: 132-143.
- [24] Nesterov SV, Han C, Maki M, Kajander S, Naum AG, Helenius H, Lisinen I, Ukkonen H, Pietila M, Joutsiniemi E and Knuuti J. Myocardial perfusion quantitation with <sup>150</sup>I-labelled water PET: high reproducibility of the new cardiac analysis software (Carimas). *Eur J Nucl Med Mol Imaging* 2009; 36: 1594-1602.
- [25] Harms HJ, Knaapen P, de Haan S, Halbmeijer R, Lammertsma AA and Lubberink M. Automatic generation of absolute myocardial blood flow images using [<sup>150</sup>]H<sub>2</sub>O and a clinical PET/CT scanner. *Eur J Nucl Med Mol Imaging* 2011; 38: 930-939.
- [26] Inaba T. Quantitative measurements of prostatic blood flow and blood volume by positron emission tomography. *J Urol* 1992; 148: 1457-1460.
- [27] Kurdziel KA, Figg WD, Carrasquillo JA, Huebsch S, Whatley M, Sellers D, Libutti SK, Pluda JM, Dahut W, Reed E and Bacharach SL. Using positron emission tomography 2-deoxy-2-[<sup>18</sup>F] fluoro-D-glucose, <sup>11</sup>C<sub>10</sub>, and <sup>150</sup>I-water for monitoring androgen independent prostate cancer. *Mol Imaging Biol* 2003; 5: 86-93.
- [28] Iida H, Rhodes CG, de Silva R, Yamamoto Y, Araujo LI, Maseri A and Jones T. Myocardial tissue fraction—correction for partial volume effects and measure of tissue viability. *J Nucl Med* 1991; 32: 2169-2175.
- [29] Cho E, Chung DJ, Yeo DM, Sohn D, Son Y, Kim T and Hahn ST. Optimal cut-off value of perfusion parameters for diagnosing prostate cancer and for assessing aggressiveness associated with Gleason score. *Clin Imaging* 2015; 39: 834-840.
- [30] Miyata Y and Sakai H. Reconsideration of the clinical and histopathological significance of angiogenesis in prostate cancer: usefulness and limitations of microvessel density measurement. *Int J Urol* 2015; 22: 806-815.
- [31] Apostolova I, Hofheinz F, Buchert R, Steffen IG, Michel R, Rosner C, Prasad V, Kohler C, Derlin T, Brenner W and Marnitz S. Combined measurement of tumor perfusion and glucose metabolism for improved tumor characterization in advanced cervical carcinoma. A PET/CT pilot study using [<sup>150</sup>]water and [<sup>18</sup>F]fluorodeoxyglucose. *Strahlenther Onkol* 2014; 190: 575-581.
- [32] Van der Veldt AA, Lubberink M, Bahce I, Walraven M, de Boer MP, Greuter HN, Hendrikse NH, Eriksson J, Windhorst AD, Postmus PE, Verheul HM, Serne EH, Lammertsma AA and Smit EF. Rapid decrease in delivery of chemotherapy to tumors after anti-VEGF therapy: implications for scheduling of anti-angiogenic drugs. *Cancer Cell* 2012; 21: 82-91.

# PET perfusion in prostate cancer



# PET perfusion in prostate cancer

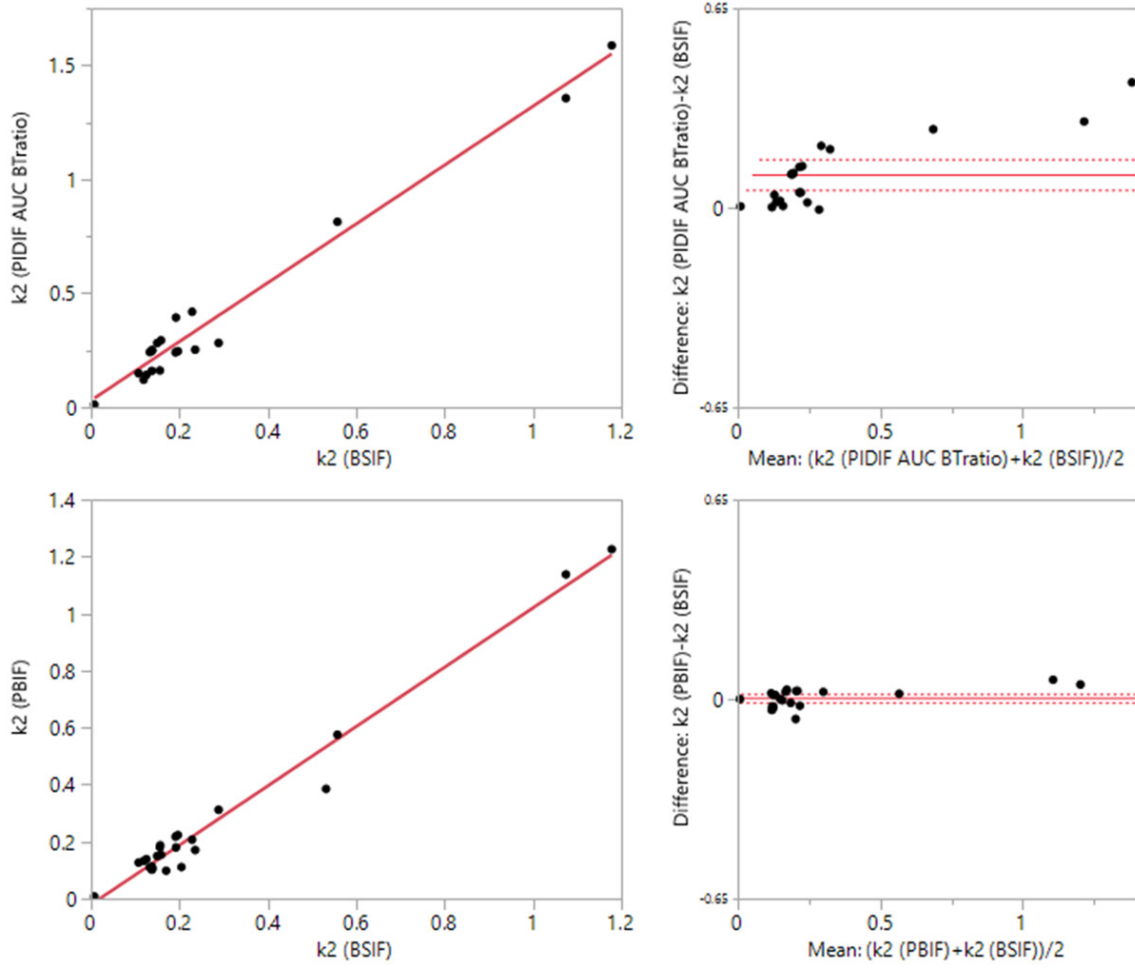
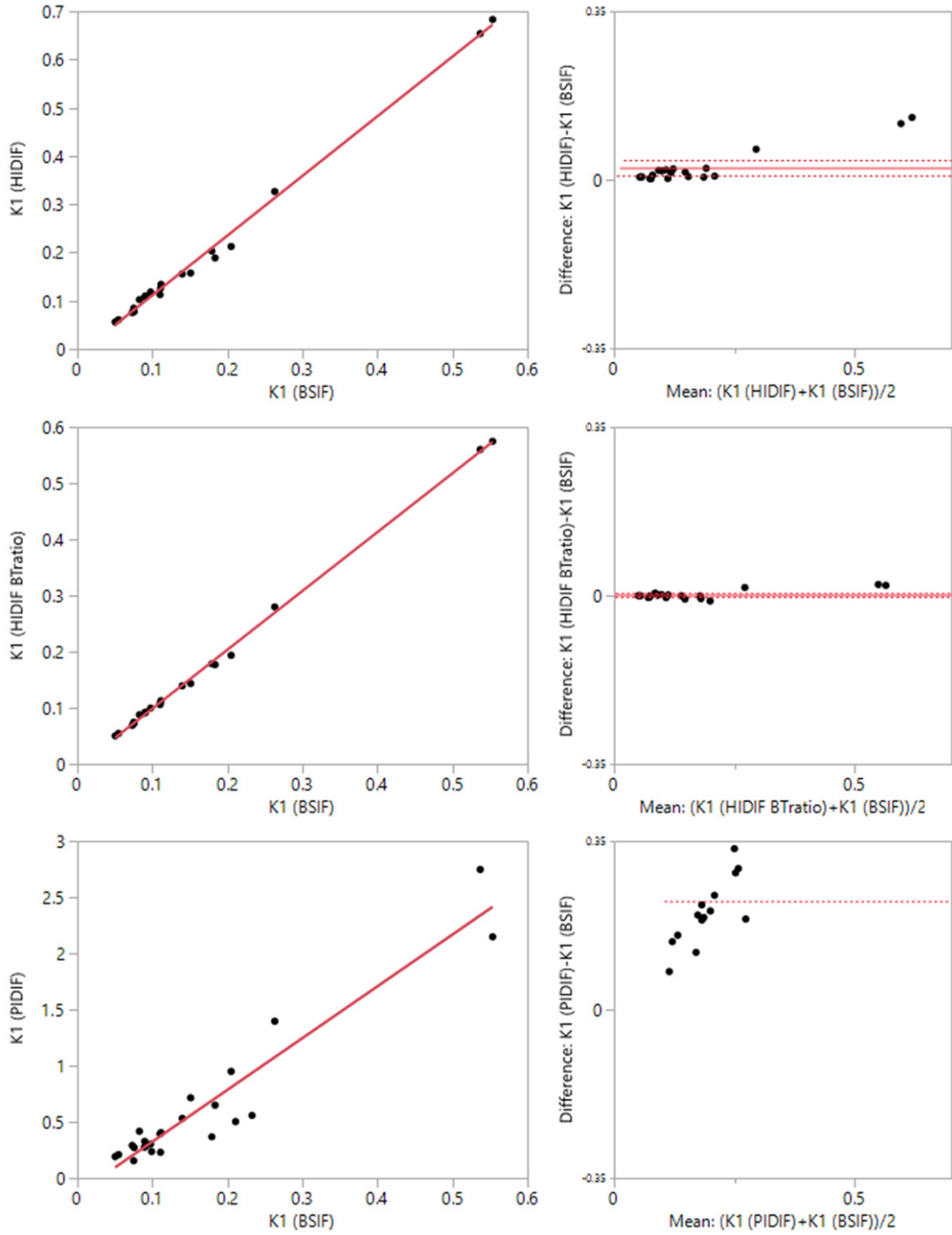


Figure S1.  $k_2$  linear regression and Bland-Altman plots for all IDIFs and PBIF compared to BSIF.

# PET perfusion in prostate cancer



PET perfusion in prostate cancer

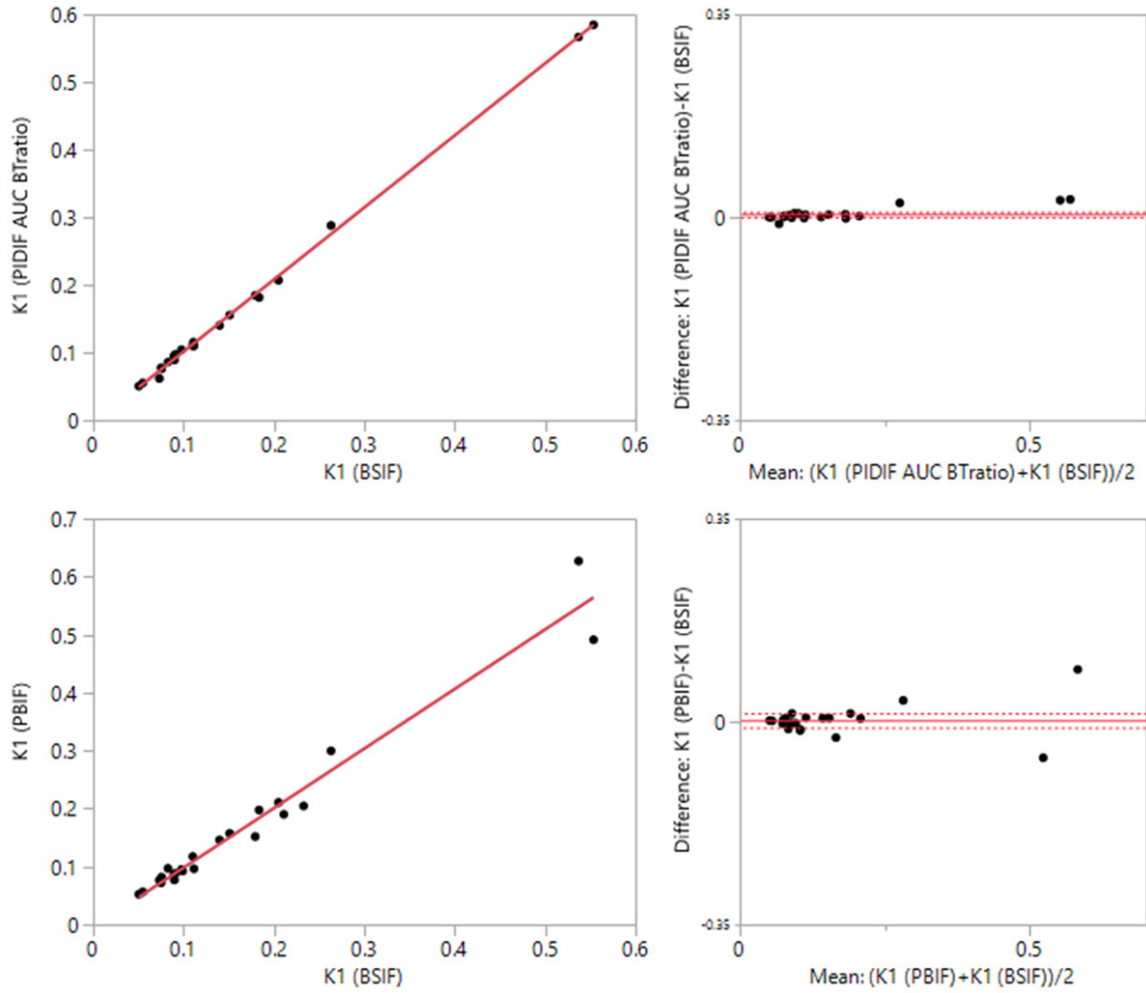


Figure S2.  $K_1$  linear regression and Bland-Altman plots for all IDIFs and PBIF compared to BSIF.

# PET perfusion in prostate cancer

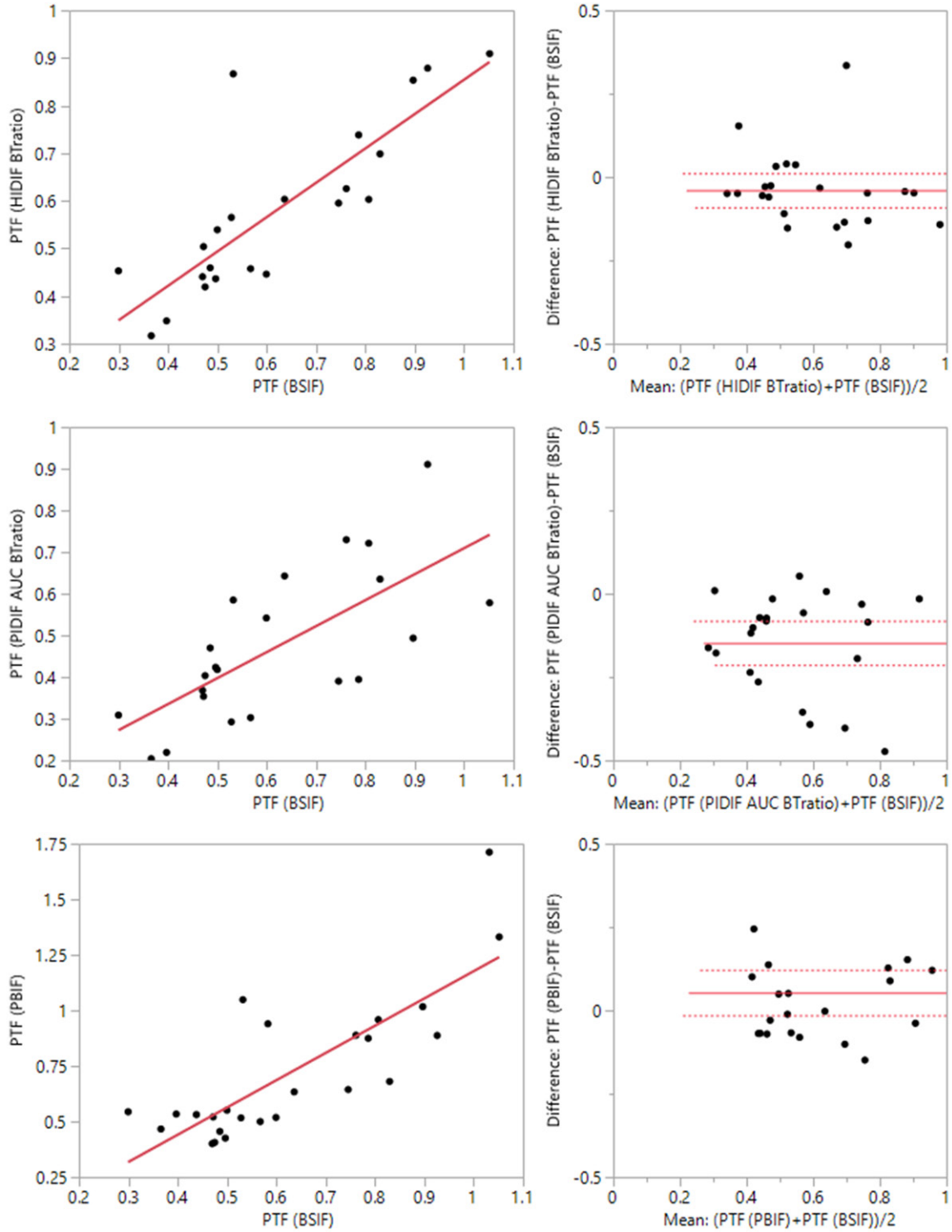
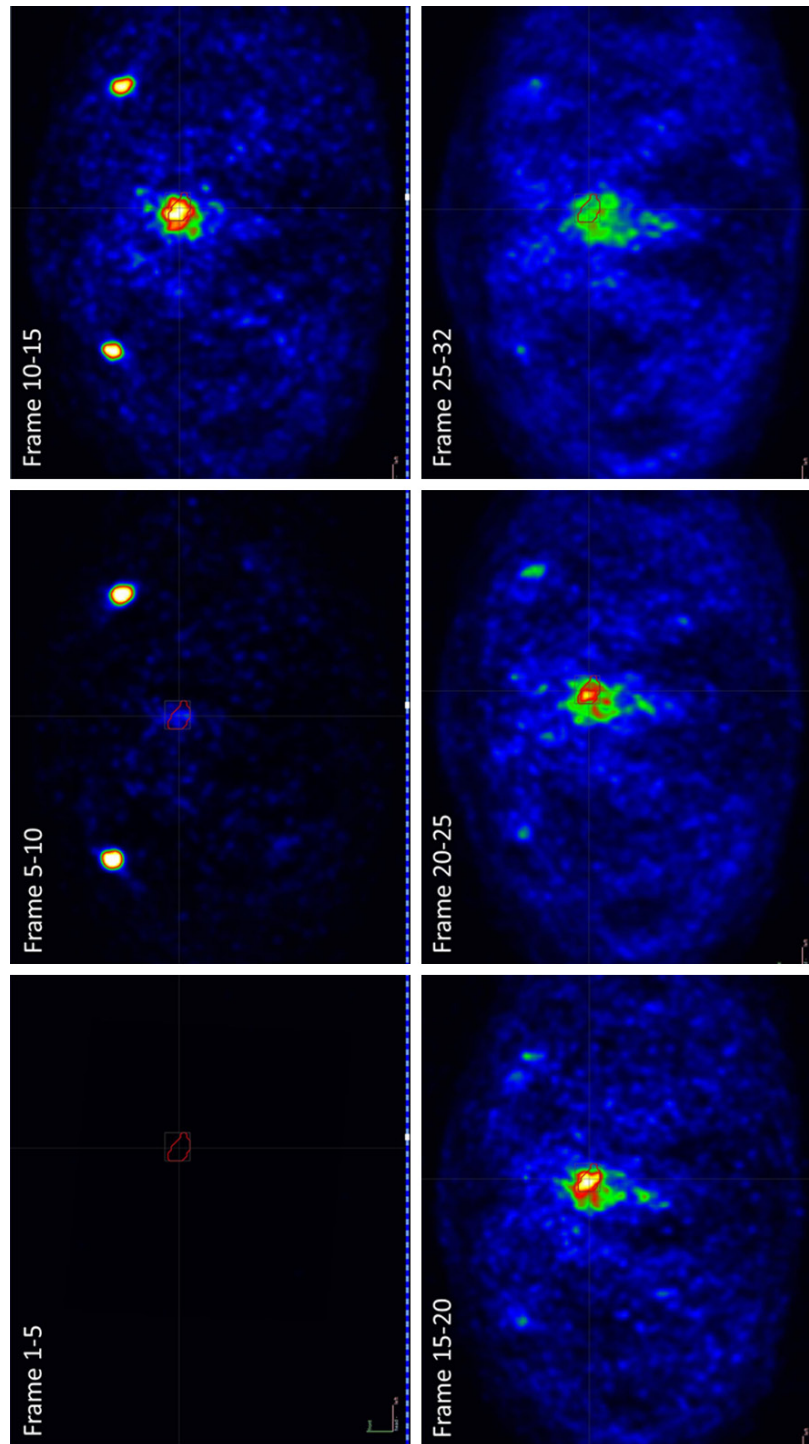


Figure S3. PTF linear regression and Bland-Altman plots for all IDIFs and PBIF compared to BSIF.

## PET perfusion in prostate cancer



**Figure S4.** Example of a dynamic PET series (patient 8) with tumor ROI outlined in red. Each image was calculated as a weighted average of the 5 (or 7) frames and the same scale (0 to 35 kBq/ml) was used.

## PET perfusion in prostate cancer

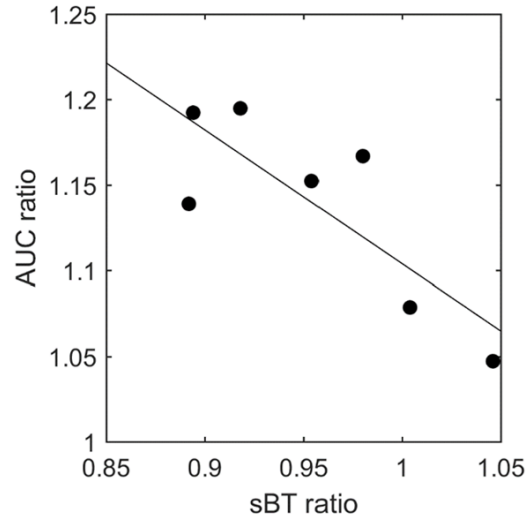


**Figure S5.** Ratio of systolic blood pressures (sBT) during the heart and pelvic scans against the ratio of the areas under the first pass curve (AUC). Solid line is a linear fit ( $0.78 \times \text{sBT ratio} + 1.89$ ,  $r=0.81$ ,  $P<0.05$ ). Approximately 2/3 of the variation of AUC is explained by the difference in sBT. Including heart rate did not improve the model. The curve was used to correct the HIDIF to the conditions during the pelvic scan.